Nature Environment and Pollution Technology
An International Quarterly Scientific Journal

p-ISSN: 0972-6268
(Print copies up to 2016)
e-ISSN: 2395-3454

Vol. 25 | No. 2 | Article ID B4379 | 2026

Original Research Paper

https://doi.org/10.46488/NEPT.2026.v25i02.B4379

Open Access Journal

# Synthesis and Adsorptive Performance of Zn/Al Dually Doped *Brassica oleracea* Var. *italica* Stem Nanocomposite: Insights from Response Surface Methodology (RSM) Optimization

**Yagna Sri Thikkada[1], Alpitha Suhasini Juttuka[2], Venkata Ramana Avula[3], NagaRaju Yendluri[1], Kapavarapu Sreekar[1], Pulipati King[1] and Meena Vangalapati[1]†**

[1]Department of Chemical Engineering, AUCE, Andhra University, Visakhapatnam, A.P., India
[2]Department of Chemical Engineering and Petroleum Engineering, UCEK, JNTUK, Kakinada, A.P., India
[3]Department of Petroleum Engineering, Godavari Global University, Rajahmundry, A.P., India
†Corresponding author: Meena Vangalapati; meenasekhar2002@yahoo.com

**Abbreviation: Nat. Env. & Poll. Technol.**
**Website: www.neptjournal.com**

*Received:* 20-07-2025
*Revised:* 04-10-2025
*Accepted:* 06-10-2025

*Key Words:*

Zn/Al dually doped nanocomposite
*Brassica oleracea* var. *italica*
Sustainable nanocomposite
Dye adsorption
RSM with a CCD

*Citation for the Paper:*

Thikkada, Y.S., Juttuka, A.S., Avula, V.R., Yendluri, N., Sreekar, K., King, P. and Vangalapati, M., 2026. Synthesis and adsorptive performance of Zn/Al dually doped Brassica oleracea var. italica stem nanocomposite: insights from response surface methodology (RSM) optimization. *Nature Environment and Pollution Technology*, 25(2), B4379. https://doi.org/10.46488/NEPT.2026.v25i02.B4379

*Note: From 2025, the journal has adopted the use of Article IDs in citations instead of traditional consecutive page numbers. Each article is now given individual page ranges starting from page 1.*



## ABSTRACT

In this study, a sustainable nanocomposite was synthesized using the stem waste of Brassica oleracea var. italica, dually doped with Zn and Al (Zn/Al@BOI), through a chemical co-precipitation method. The material was designed for the efficient adsorptive treatment of wastewater to remove Malachite Green (MG). The structural and surface features were analyzed using SEM, BET, EDX, XRD, FTIR, XPS, and TGA. The presence of Zn and Al was confirmed by EDX and XPS, while BET surface area analysis confirmed a notably high value of 80.53 $m^2.g^{-1}$, suggesting the strong adsorption capability of the material. To investigate its adsorption behavior, a set of batch tests was conducted, focusing on the influence of time, pH, adsorbent dose, MG dye concentration, and temperature. Using RSM with a CCD, the ideal operational conditions were determined to be approximately 29.64 min of contact time, 0.29 $g.L^{-1}$ dosage, pH 7.96, and 20 ppm dye concentration, resulting in a greater efficiency of 97.31%. The equilibrium data best fit the Freundlich isotherm ($R^2$ = 0.9957), while the Langmuir model analysis revealed a monolayer capacity of 336 mg. $g^{-1}$. The adsorption kinetics were effectively represented by the pseudo-2$^{nd}$-order model, and the thermodynamic findings revealed a spontaneous, endothermic, and physisorption-driven process.

## INTRODUCTION

The issue of water pollution is particularly relevant when it arises from industrial sources such as dye effluents, as it can have dire consequences and pose serious risks to both environmental and human well-being (Sowjanya et al. 2023). Contaminated water from the textile, leather, and paper industries is a major environmental concern because it discharges synthetic dyes such as MG, which are non-biodegradable, toxic, and persistent (Raval et al. 2017). Malachite Green ($C_{23}H_{25}ClN_2$), widely used in textile industries and aquaculture, is a clear example, as it is a synthetic dye with strong color and chemical stability. Its complex molecular structure renders it toxic, environmentally resistant, and resistant to biodegradation (Verma et al. 2020). The accumulation of dyes in aquatic systems endangers the environment and human health; therefore, stringent policies are needed alongside effective removal strategies (Shindhal et al. 2021). Adsorption is regarded as one of the most efficient methods among those studied, including photocatalysis, coagulation-flocculation, chemical oxidation, and membrane filtration, because of its operational ease, low cost, high efficacy even at low concentrations, and lack of harmful by-products (Inobeme et al. 2024, Dutta et al. 2021). These factors have made it increasingly favorable in recent years (Bilal et al. 2022).

In recent years, researchers have increasingly explored nanomaterial-based adsorbents because of their exceptionally large surface areas, high chemical reactivity, and strong ability to bind with various pollutants (Zhang et al. 2022). One of the key applications of such materials is to address synthetic dye contamination in industrial liquid waste. The use of sustainable, bio-waste-derived nanocomposites has become increasingly prominent, particularly those doped with metals, which combine cost-effectiveness and environmental safety (Jha et al. 2024). The advancement of nanotechnology has enabled the fabrication of high-performance adsorbents with better selectivity, recyclability, and efficiency, making them highly suitable for broader wastewater treatment applications (Granado et al. 2024).

Among bio-derived materials, agricultural and food-processing wastes are particularly noteworthy due to their affordability, widespread availability, and environmentally sustainable nature. When doped with metals such as Zn, Al, Fe, Ti, Mn, Co, Ni, Ag, and Cu, these wastes can be transformed into efficient adsorbents with improved porosity and active surface sites. Several studies have demonstrated the utility of materials synthesized via green routes. For instance, Cifci et al. (2022) explored the use of iron-doped coffee waste as a low-cost solution for capturing Reactive Blue 21 dye, presenting an innovative reuse of food waste. Manoj Kumar et al. (2023) synthesized ZnO nanoparticles using Brassica oleracea var. botrytis (cauliflower) leaf extract via a co-precipitation method, promoting plant-based synthesis of AgNPs. Similarly, Ananda et al. (2023) employed Basella alba leaf juice in the combustion synthesis of $2ZrO_2$–$7ZnO$ nanoparticles, and Ashraf et al. (2023) used amla seed extract to green-synthesize iron oxide nanoparticles with enhanced biological compatibility.

Other notable examples include the fabrication of aluminum-doped cadmium oxide cathodes using plasma-treated peanut shell-derived carbon for energy storage systems (Karthikeyan et al. 2024) and the synthesis of zinc-doped hydroxyapatite nanorods from scallop shell waste for potential biomedical applications (Karunakaran et al. 2023). These examples highlight the broad versatility of metal-doped bio-waste-derived materials across the environmental, biomedical, and energy sectors.

Recent advances in green chemistry further support the use of dually doped systems, where two metals are integrated into biomass matrices, to enhance adsorption efficiency. This strategy enhances the surface reactivity, active site availability, and overall performance. Chan et al. (2020), for example, developed ZnO nanoparticles dually doped with Fe and Ag using Clitoria ternatea extract, achieving a 97.4% removal of Congo red. Velusamy et al. (2025) prepared a Ni/Al-layered double hydroxide (LDH) through neem-assisted co-precipitation that removed more than 95% of methylene blue dye. Ouadrhiri et al. (2022) reported the development of an N, P dually doped carbon catalyst from olive pomace, capable of degrading 94.6% of methyl orange through persulfate-assisted oxidation. Mohan Raj et al. (2023) introduced a novel composite material, [EDA-OPDA] Al@Zn, by coating aluminum with a copolymer and then incorporating zinc via electrodeposition, showcasing the adaptability of metal dually doping approaches.

Given the increasing focus on sustainable water treatment, dual doping of bio-waste with metals such as Zn and Al, especially in biomass such as Brassica oleracea stems (found in broccoli, cabbage, and cauliflower), has been shown to significantly improve porosity, functional group density, and adsorption affinity. Building on this, the current study focuses on the eco-friendly fabrication of a Zn/Al dual-doped nanocomposite (Zn/Al@BOI) using Brassica oleracea var. italica (broccoli) stem waste, using a simple chemical co-precipitation method. This environmentally friendly process avoids hazardous reagents and promotes sustainability in chemistry by repurposing agricultural waste. The nanocomposite was effectively utilized to treat wastewater and remove Malachite Green (MG). Its structural and surface activity were thoroughly examined using SEM-EDX, XRD, BET, FTIR, and TGA, all of which confirmed successful metal incorporation and a favorable surface morphology. To evaluate its adsorption behavior, batch experiments were conducted under varying conditions of contact time, adsorbent dosage, dye concentration, temperature, and pH. The adsorption mechanism was further explored using isotherm, kinetic, and thermodynamic models. For process optimization, (RSM) using a Central Composite Design (CCD) was utilized to determine the most effective operating variables. The nanocomposite exhibited a high removal efficiency even under real wastewater conditions, underscoring its potential as a sustainable and effective adsorbent for dye remediation.

## MATERIALS AND METHODS

### Materials

$ZnCl_2$, $Al_2O_3$, Triton X-100, sodium hydroxide (NaOH) pellets, MG dye, and DI water were procured from the Andhra Scientific Agency, Kakinada, India. Stems of *Brassica oleracea* var. *italica* were collected from the vegetable market in Kakinada, India.

### Preparation of *Brassica oleracea* var. *italica* Stem Powder

The stems were rinsed extensively with distilled water to

eliminate surface contaminants and impurities. They were chopped into smaller pieces and left to dry naturally in the sunlight for four days. The samples were then placed in an oven at 70°C for 12 h to achieve total dehydration. Once dried, the material was finely ground and passed through a 100-mesh (150 µm) sieve to achieve a consistent powder, which was then stored in sealed containers for later use in synthesizing the nanocomposite (Granado et al. 2024).

**Selection of Zn:Al Ratio**

A Zn-to-Al molar ratio of 2:1 was chosen for synthesizing the Zn/Al@BOI nanocomposite to balance surface reactivity and structural stability. This ratio is supported by the literature, which indicates that moderate zinc enrichment improves ZnO dispersion, enhances active site density, and boosts adsorption efficiency. Higher ratios (e.g., 3:1) may cause Zn agglomeration and reduce the surface area, whereas lower ratios (e.g., 1:1 or 1:2) could limit $Zn^{2+}$ availability, which is essential for dye interaction. Thus, the 2:1 ratio offers an optimal composition for developing a porous, metal-rich, and stable adsorbent for aqueous media (Ouassif et al. 2020, Tajat et al. 2022, Youssef et al. 2017).

**Preparation of Zn/Al@BOI Nanocomposite**

A sustainable Zn/Al@BOI nanocomposite was prepared using 20 g of dried, powdered *Brassica oleracea* var. *italica* biomass via co-precipitation and calcination (Fig. 1). The biomass was stirred into 200 mL of distilled water to ensure uniform dispersion. Zinc chloride and aluminum chloride hexahydrate (0.5 M each) were added in a Zinc and Al molar ratio of 2:1 to enhance structural stability and adsorption efficiency (Youssef et al. 2017). To control particle size and dispersion, 1 g of Triton X-100 was introduced. The prepared metal salt solution was gradually added dropwise to the biomass suspension while continuously stirring, and the pH was carefully regulated to 10 using NaOH to initiate the co-precipitation process. The mixture was heated at 70 °C with continuous stirring for 3 h and then allowed to stand at room temperature for 24 h. The formed solid was filtered, washed with distilled water until the pH was neutral, and dried in an oven at 80 °C for 12 h. To enhance the crystallinity and stability, the dried material was calcined at 450°C for 3 h to form stable metal oxides with improved crystallinities and surface activities (Velusamy et al. 2025, Ouadhriri et al. 2022, Ouassif et al. 2020).

**Batch Mode Adsorption Tests**

Adsorption experiments were conducted by systematically varying key parameters, including the treatment time, nanocomposite dose ($g.L^{-1}$), pH, and MG dye concentration ($mg.L^{-1}$). The prepared dye-adsorbent mixtures were shaken using an orbital shaker with temperature control for predetermined time intervals. Post-agitation, centrifugation was performed at 4000 rpm for 15 min to achieve phase separation. The concentration of unabsorbed dye in the liquid phase was quantified using UV–Visible spectroscopy at 618 nm, employing a 1 cm quartz cuvette. The pH of the solutions was monitored using a calibrated digital pH meter (Sowjanya et al. 2023, Ratnam et al. 2022, Subhashita et al. 2022). The % removal was determined according to Equation (1) and the equilibrium uptake of dye by the adsorbent ($q_e$, $mg.g^{-1}$), which indicates the quantity of MG dye retained per gram of adsorbent at equilibrium, according to Equation (2):

$$\% \text{ Removal efficiency} = \frac{C_o - C_e}{C_o} \times 100 \quad \ldots(1)$$


Fig. 1: Overview of the synthetic route used to prepare the Zn/Al@BOI nanocomposite.

$$\text{Dye uptake} = (C_o - C_e) \times \frac{V}{m} \quad \ldots(2)$$

Here, $C_o$ and $C_e$ correspond to the MG concentrations at the beginning and equilibrium ($mg.L^{-1}$), respectively, V is the solution volume in liters, and m denotes the amount of adsorbent in grams.

**Isotherm, Kinetic and Thermodynamic Studies**

Equilibrium adsorption studies are essential for understanding both the capacity of the nanocomposite and the nature of its binding to dye molecules. In this study, the adsorption behavior of MG onto the Zn/Al@BOI nanocomposite was assessed using two well-established isotherm models: Langmuir and Freundlich. The Langmuir model describes monolayer coverage on an even surface with identical and fixed adsorption sites, whereas the Freundlich model is empirical and describes adsorption on uneven surfaces with sites of different binding strengths. The corresponding mathematical expressions for these models are presented in Equations (3) and (4) (Sowjanya et al. 2023, Ratnam et al. 2022, Subhashita et al. 2022). The following equation outlines the Langmuir model (Eq. 3) and the Freundlich adsorption isotherm (Eq. 4):

$$\frac{C_e}{q_e} = \left(\frac{C_e}{q_{max.}}\right) + \frac{1}{q_{max.}.b} \quad \ldots(3)$$

$$\ln q_e = \ln K_f + \frac{1}{n} \ln C_e \quad \ldots(4)$$

In this equation, $q_{max}$ represents the maximum amount of dye that can be adsorbed per unit mass of the adsorbent ($mg.g^{-1}$), and b corresponds to the Langmuir constant related to adsorption affinity (L/mg). In the Freundlich model, the constants $K_f$ and n correspond to the dye uptake and absorbance of adsorption, respectively, indicating surface heterogeneity.

Kinetic models are useful for analyzing adsorption rates and determining the rate-controlling mechanisms. In this work, the adsorption kinetics of MG onto Zn/Al@BOI nanocomposite were assessed using pseudo-1st order, pseudo-2nd order, Elovich, and intra-particle diffusion models to describe the interaction dynamics between dye molecules and the adsorbent surface (Subhashita et al. 2022, Ho et al. 1999, Debord et al. 2022, Dharmarathna et al. 2024). The mathematical equations of Pseudo first (Eq. 5) and second-order (Eq. 6) kinetic models:

$$\ln(q_e - q) = -K_1 t + \ln q_e \quad \ldots(5)$$

$$\frac{t}{q} = \left(\frac{1}{q_e}\right) t + \left(\frac{1}{K_2}.\frac{1}{q_e^2}\right) \quad \ldots(6)$$

Here, $q_e$ ($mg.g^{-1}$) is defined as the equilibrium concentration of MG dye adsorbed on one gram of the adsorbent, indicating the adsorption capacity of the system. The term $q_t$ (mg/g) denotes the dye uptake at a specific time, t. $K_1$ and $K_2$ represent the rate constants for the pseudo-first- and second-order models, respectively, with units of $1.min^{-1}$ and $g/(mg \cdot min^{-1})$ and are used to describe the adsorption rate and underlying kinetics.

Adsorption behavior is closely linked to thermodynamic parameters such as Gibbs free energy (ΔG°), enthalpy (ΔH°), and entropy (ΔS°), revealing its spontaneity, thermal behavior, and level of randomness between the solid and liquid phases. These values are determined using the distribution coefficient ($K_c$), and calculated through temperature-dependent relationships, typically employing the Van't Hoff equation (Sowjanya et al. 2023, Ratnam et al. 2022, Subhashita et al. 2022).

$$\Delta G^o = -RT \ln K_c \quad \ldots(7)$$

$$K_c = \frac{q_e}{C_e} \quad \ldots(8)$$

$$\ln K_c = -\frac{\Delta H^0}{RT} + \frac{\Delta S^0}{R} \quad \ldots(9)$$

where T is the absolute temperature (K), R is the universal gas constant (8.314 $J \cdot mol^{-1} \cdot K^{-1}$), $C_e$ (mg/L) is the equilibrium dye concentration, and $q_e$ ($mg.g^{-1}$) represents the amount of dye adsorbed at equilibrium.

**RSM (Response Surface Methodology)**

RSM is a powerful tool combining numerical modelling approaches to analyze experimental data, assess variable interactions, and develop predictive models (Sowjanya et al. 2023, Poiba et al. 2023, Polipalli et al. 2013). Among its designs, the Central Composite Design (CCD) is widely used for process optimization, as it can estimate linear, quadratic, and interaction effects without compromising model reliability. CCD employs axial (star) points outside the factorial cube, maintaining uniform prediction accuracy around the center point. In this study, preliminary screening was used to identify suitable parameter ranges. CCD was used to optimize four parameters: stirring time (A), adsorbent dose (B), pH (C), and adsorbate concentration (D). A second-order polynomial model was generated in Design Expert 13 to predict the efficiency (Table 1).

Table 1: Factors affecting optimization.

| Factors | Units | Min (-1) | Max (+1) |
|---|---|---|---|
| A-Time | min | 10.00 | 50.00 |
| B-Dosage | $g.L^{-1}$ | 0.10 | 0.50 |
| C-pH | | 6.00 | 10.00 |
| D-Concentation | $mg.L^{-1}$ | 10.00 | 30.00 |

## RESULTS AND DISCUSSION

### Characterization of the Adsorbent

The SEM image (Fig. 2a) reveals that the Zn/Al@BOI nanocomposite exhibits a distinct layered morphology with a nanoflake-like appearance. These structures appeared as irregularly shaped aggregated sheets, suggesting the successful formation of a porous and interconnected network. Such morphology is advantageous for adsorption, as it offers enhanced surface area and large accessible active sites, and the particle sizes observed in the micrograph ranged from 47.10 to 64.49 nm, confirming the nanoscale dimension of the synthesized material. This structural arrangement is consistent with the typical lamellar morphologies observed in layered double hydroxide-based nanomaterials, further supporting the effective incorporation of Zn and Al into the biomass matrix. The loose, porous arrangement of the flakes suggests a high surface area with numerous accessible active sites, making the material well-suited for adsorption applications (Aziz et al. 2023, Javadian et al. 2014, Mall et al. 2006).

Elemental composition analyzed via EDX (Fig. 2b) revealed the dominant presence of carbon, oxygen, zinc, and aluminum, which together accounted for approximately 92–94 wt. %, which forms the backbone of the nanocomposite. Additional elements such as sodium, potassium, calcium, phosphorus, and trace chlorine were also detected, likely originating from the biomass source or residual precursors such as $ZnCl_2$ and $AlCl_3$, indicating that the washing process was effective (Sowjanya et al. 2022).

The XRD patterns (Fig. 2c) exhibited well-defined peaks at 2θ values of 32.1°, 34.0°, 36.2°, 48.3°, 57.1°, 63.6°, 66.1°, and 68.1°, which were indexed to the (100), (001), (101), (102), (103), (110), (200), and (112) planes of hexagonal wurtzite ZnO, confirming its crystalline phase. The broadening of the peaks suggests the presence of nanocrystalline domains and possible lattice distortion due to $Al^{3+}$ incorporation. These findings collectively confirm the successful formation of crystalline Zn/Al@BOI nanocomposites with surface and structural features that are highly favorable for adsorption processes (Banerjee et al. 2017, Klett et al. 2014).

The FT-IR spectra of the Zn/Al@BOI nanocomposite before and after MG removal are shown in Fig. 3(a) and 3(b), respectively. Prior to adsorption, characteristic peaks were identified at 3420.17 $cm^{-1}$, 2923.88 $cm^{-1}$, and 1630.64 $cm^{-1}$, likely due to H-O-H bending or C=O vibrational stretching modes. Additional signals at 1382.24 $cm^{-1}$ (–$CH_3$ bending) and 1026.74 $cm^{-1}$ (C=O stretching) were observed, alongside lower-frequency bands at 876.32, 617.29, and 466.65 $cm^{-1}$, corresponding to C–H bending and metal–oxygen (Zn–O and Al–O) vibrational modes. After the adsorption of the MG dye, notable spectral changes occurred. The broad O–H band near 3420 $cm^{-1}$ decreased in intensity and shifted slightly, suggesting hydrogen bonding or interactions with the dye molecules. The peak at 1630.64 $cm^{-1}$ became more pronounced, possibly due to the aromatic C=C stretching or N–H bending vibrations introduced by the dye. Reductions in the 1382 and 1026 $cm^{-1}$ bands indicated the participation of –$CH_3$ and C-O groups in adsorption. Additionally, the weakening of the metal–oxygen vibrational bands below 700 $cm^{-1}$ suggests surface interactions or coverage by MG dye molecules. These spectral modifications indicate both physical and chemical adsorption mechanisms (Sowjanya et al. 2022, Elizalde et al. 2006, Parveen et al. 2018).

To explore the surface chemistry of Zn/Al@BOI, XPS analysis was conducted. The full-range XPS scan (Fig. 4a) revealed the presence of C 1s (49.2%), O 1s (42.4%), Zn $2p_3$ (5.6%), Al 2p (2.7%), and trace Cl 2p (<0.1%), confirming the elemental composition of the material. High carbon and oxygen content reflect the biomass origin and surface metal oxide formation. The C 1s spectrum (Fig. 4b) showed a primary peak at 285.1 eV (C–C/C–H) and a shoulder at 286.2 eV (C–O). The O1s spectrum (Fig. 4c) displayed peaks at 531.2 eV (Zn–O/Al–O) and 532.6 eV ($OH^-$ or adsorbed oxygen). The Zn 2p peaks at 1021.9 eV and 1044.9 eV (Fig. 4d) confirmed $Zn^{2+}$ as ZnO, while the Al 2p signal at 74.3 eV (Fig. 4e) indicated $Al^{3+}$ in $Al_2O_3$, consistent with the values reported by Liu et al. (2019). These findings confirm the incorporation of Zn and Al, along with oxygen-containing groups.

The thermal behavior of the Zn/Al@BOI nanocomposite was evaluated using TGA, DTG, and DTA analyses (Fig. 5a–b). The TGA curve exhibited three main steps in mass loss. The preliminary weight loss of approximately 4.3% below 150°C was attributed to the release of physically adsorbed volatile water from the samples. Between 150–300°C, a significant mass reduction of around 15.0% occurred, which was attributed to the decomposition of organic components, such as cellulose and other plant-based residues. Beyond 300°C, a gradual mass reduction continued to 600°C, primarily due to the breakdown of residual organics and the dehydroxylation of Zn and Al hydroxides. The DTG peak centered near 250°C marked the primary decomposition stage, which was aligned with a strong endothermic signal in the DTA curve. Overall, a total mass loss of approximately 18.3% was observed, suggesting moderate organic content in the material. The remaining mass (~81.7%) reflects high thermal stability and indicates the presence of thermally robust metal-oxides such as ZnO and $Al_2O_3$ within the

composite structure (Monvisade et al. 2009, Li et al. 2018).

The porous structure of Zn/Al@BOI was further examined via nitrogen adsorption–desorption analysis (Fig. 6a–b). The isotherm manifested a Type IV pattern with an H3 loop in the relative pressure of $P/P_0 \approx 0.8–1.0$, typical of mesoporous materials with slit-like pores, often found in layered composites. A sharp uptake at $P/P_0$ close to 1.0 indicates capillary condensation within the mesopores. The BJH pore size distribution (Fig. 6b) showed a dominant average pore size of ~3.77 nm, alongside a broader range between 20–60 nm, which may result from interparticle voids or larger mesopores. The BET surface area was measured to be 80.53 $m^2.g^{-1}$, with a total pore volume of 0.186 $cm^3.g^{-1}$. These properties imply high surface availability and effective pore diffusion pathways, making the composite well suited for dye adsorption applications. The summarized data in Table 2 underscore its mesoporous nature and adsorption efficiency (Kacan et al. 2016, Naeem et al. 2022).

Table 2: BET results of Zn/Al@BOI.

| Parameter | Value | Method |
|---|---|---|
| BET area in $m^2.g^{-1}$ | 80.53 | BET method |
| Total pore volume in $cm^3.g^{-1}$ | 0.186 | BJH desorption |
| Average pore diameter in nm | 3.77 | BJH desorption (Dv(d)) |
| type of Isotherm | Type IV | IUPAC classification |
| Hysteresis loop | H3 | Indicates slit-shaped pores |
| Main pore size range [nm] | 2–10 | BJH desorption curve |
| Secondary pore range [nm] | 20–60 | Interparticle voids |

**Batch Adsorptive Investigations**

The adsorptive performance of the Zn/Al@BOI nanocomposite toward Malachite Green (MG) dye was systematically investigated by evaluating the influence of key operational parameters. In each set of experiments, one parameter was varied while the others were maintained constant, ensuring a clear understanding of its individual impact and facilitating the determination of optimal adsorption conditions (Sowjanya et al. 2023, Ratnam et al. 2022). As mentioned in Fig. 7a, time-dependent behavior was examined under fixed conditions of pH-7, temperature-303 K, and nanocomposite dosage 0.4 $g.L^{-1}$. A rapid rise occurred during the initial phase in 30 min, which gradually plateaued, indicating the attainment of adsorption equilibrium. The rapid initial uptake is attributed to the abundance of sorption sites on the adsorbent, which become occupied over time, thereby slowing the adsorption rate. As time progressed, site saturation led to a slower adsorption rate. The highest removal efficiency, approximately 84.1% for 20 $mg.L^{-1}$ of MG solution, was recorded at 30 m. Therefore, it was chosen as the benchmark shaking time for the further tests.

Fig. 7b illustrates the influence of nanocomposite dosage (0.08 to 0.6 $g.L^{-1}$) at fixed pH-7, temperature-303 K, and time-30 min. The % improved with increasing dosage owing to the presence of numerous binding regions. The highest efficiency was achieved at 0.28 $g.L^{-1}$, reaching 84.1% for 20 $mg.L^{-1}$ MG. Beyond this point, further increases in dosage showed negligible improvements, likely due to particle agglomeration or overlapping of active sites, which can reduce the effective surface area. Hence, 0.28 $g.L^{-1}$ was deemed the optimum dosage level. The role of pH was investigated by varying it from 2 to 9 (Fig. 7c), while keeping the temperature, contact time, and dosage constant at 303 K, 30 min, and 0.28 $g.L^{-1}$, respectively. The efficiency improved notably as the pH increased, reaching a maximum of 86.3% at a pH of 8 for 20 $mg.L^{-1}$ of MG. This trend is attributed to the reduced competition from $H^+$ ions at higher pH levels and the enhanced electrostatic attraction between the negatively charged Zn/Al@BOI surface and cationic adsorbate. However, at lower pH values, excess $H^+$ ions compete with dye molecules for active sites, reducing the adsorption efficiency. Thus, pH 8 was identified as the optimum pH for further studies.

The effect of temperature on adsorbate removal by Zn/Al@BOI was studied under optimal conditions—pH 8, 30 min contact time, and an optimum dosage level of 0.28 $g.L^{-1}$ (Fig. 7d). As the temperature increased from 298 K to 318 K, the adsorbate MG removal efficiency increased from 76.3% to 88.7% for a for 20 $mg.L^{-1}$ MG solution of MG. This improvement in the adsorption efficiency confirmed the endothermic nature of the process. Elevated temperatures facilitate dye diffusion by reducing the solution viscosity and enhancing molecular mobility, which, in turn, improves penetration into mesoporous structures. Moreover, the increased thermal energy helps to overcome the activation energy barrier associated with dye–surface interactions. Hence, 318 K was identified as the optimum temperature and was used for subsequent thermodynamic analysis.

Fig. 7e illustrates how varying the adsorbate MG concentration (10–100 $mg.L^{-1}$) affects both the removal % and the adsorbate uptake ($q_e$), using the optimized conditions (pH 8, 318 K, 30 min, 0.28 $g.L^{-1}$). As MG concentration increased, removal efficiency gradually declined—from approximately 98% at 10 $mg.L^{-1}$ to around 85% at 100 $mg.L^{-1}$ owing to the saturation of available active binding regions. Conversely, the adsorption capacity increased significantly from ~49 $mg.g^{-1}$ to ~396 $mg.g^{-1}$, reflecting enhanced mass transfer and dye availability at higher dye concentrations. This inverse

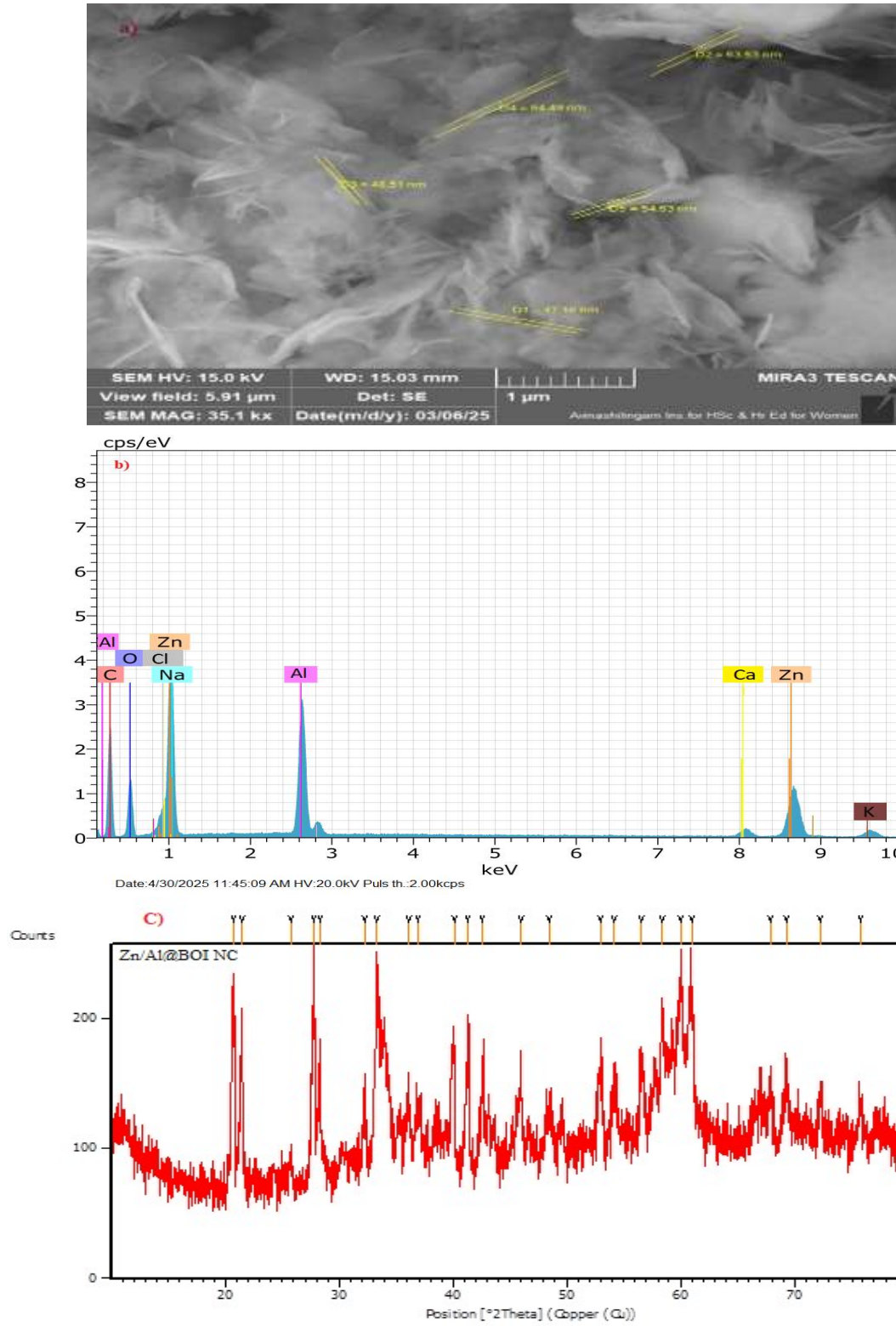


Fig. 2: (a) SEM, (b) EDX spectrum, and (c) XRD pattern of the Zn/Al@BOI nanocomposite.

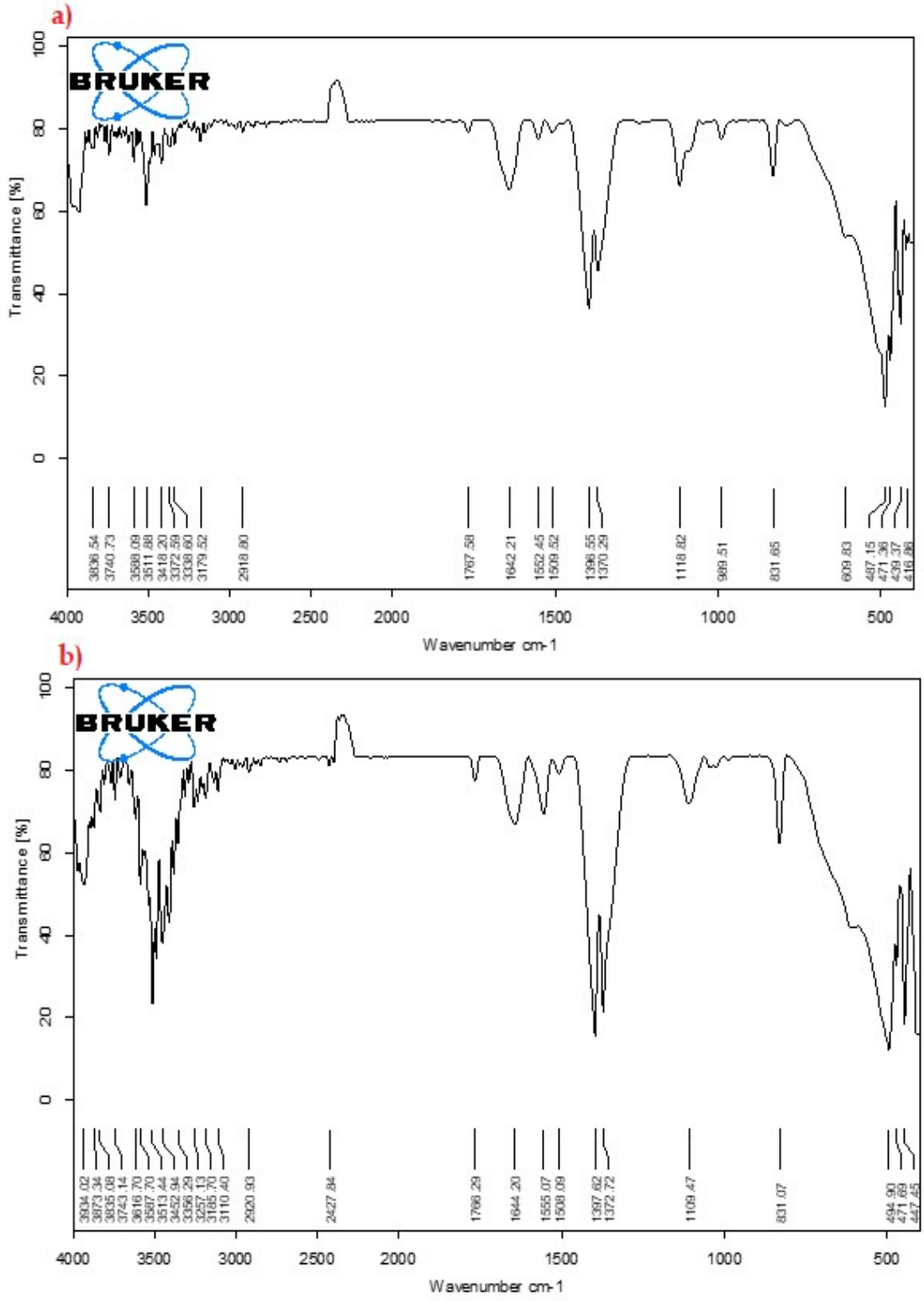


Fig. 3: FTIR profile of Zn/Al@BOI (a) before, (b) after MG dye adsorption.

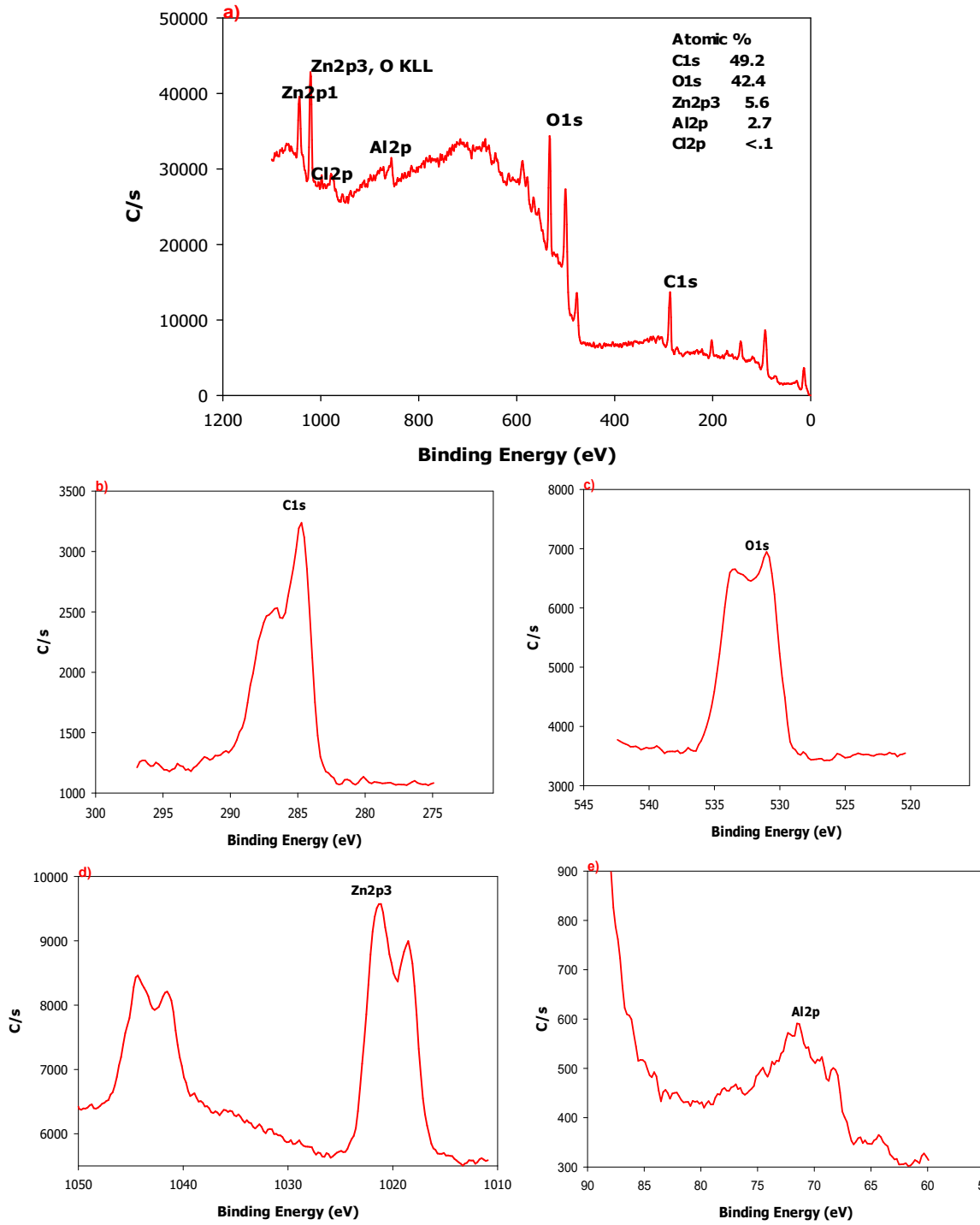


Fig. 4: XPS of Zn/Al@BOI. (a) Full range spectrum, (b) C1s, (c) O 1s, (d) Zn2p, (e) Al2p.

relationship suggests that although low concentrations are optimal for high removal efficiency, higher concentrations boost the material's uptake capacity. These outcomes highlight the importance of tuning the dye concentration for specific treatment goals and system requirements.

## RSM Outcomes

A CCD involving 31 experimental runs was employed to systematically optimize the removal of the MG dye by the Zn/Al@BOI nanocomposite. This design enabled the

investigation of four critical factors, namely shaker time (A), nanocomposite dose (B), pH (C), and adsorbate MG concentration (D), to understand both their individual and combined influences on efficiency. Experimental replicates were incorporated to ensure statistical reliability and to reduce variability. The validity and significance of the model were evaluated using analysis of variance (ANOVA), with Fisher's F-test adopted to assess statistical relevance. The predictive accuracy was determined by $R^2$, which measures how effectively the model captures the variability in the observed data. Table 3 presents the actual and coded values of all variables, along with the experimental results. The fitted quadratic regression equation, developed using the coded values of the variables, is presented as follows:

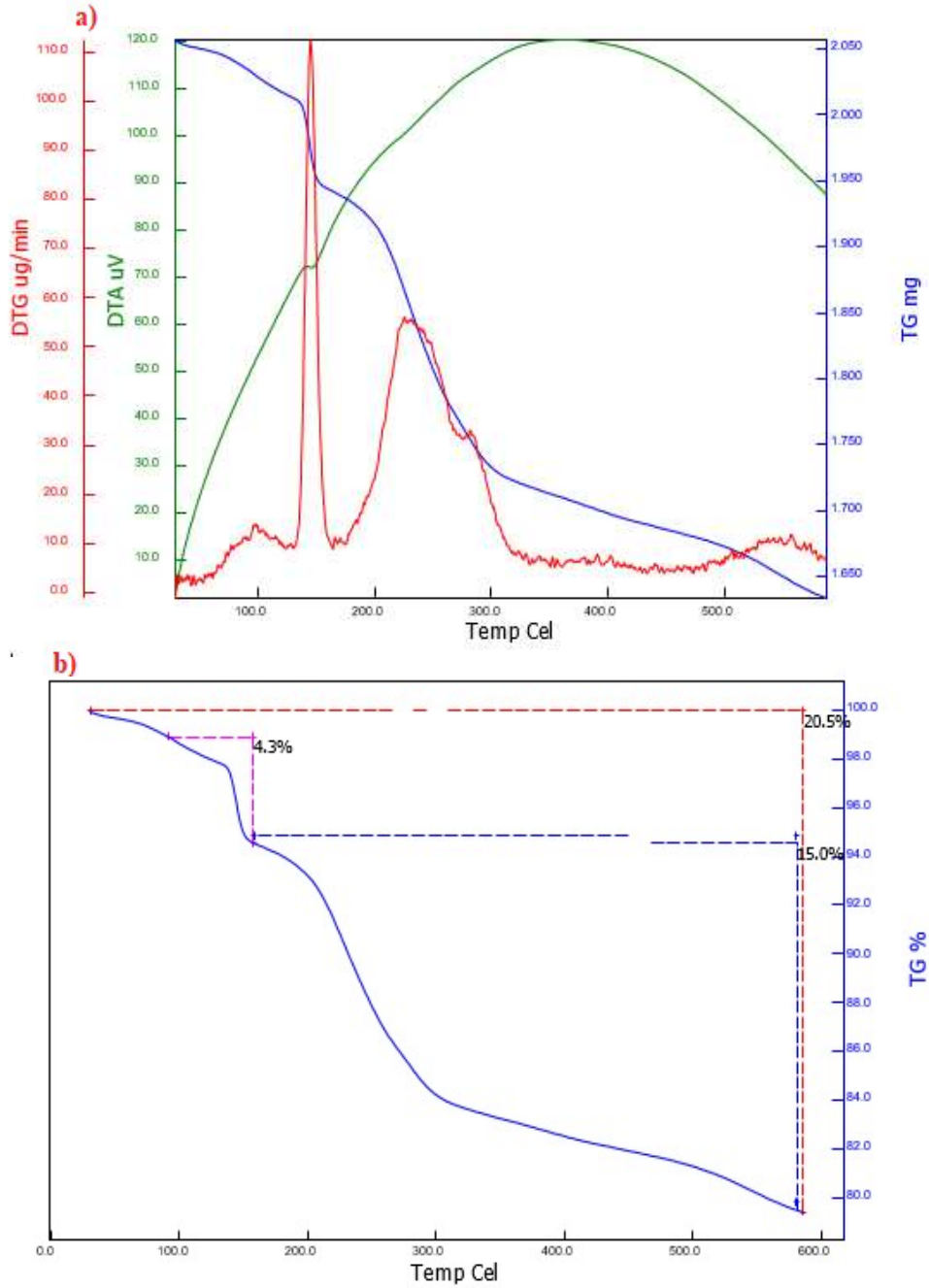


Fig. 5: (a) TGA–DTG–DTA plots and (B) TG curve of the Zn/Al@BOI nanocomposite.

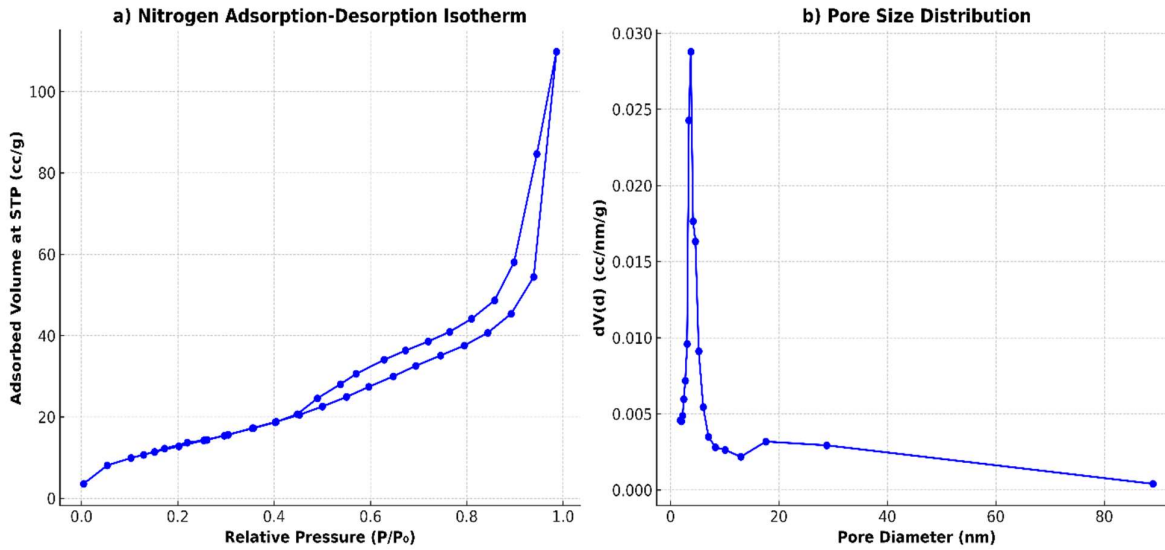


Fig. 6: Surface area and porosity analysis of Zn/Al@BOI: (a) nitrogen sorption isotherm (BET), (b) BJH pore size distribution curve.

MG removal efficiency % = 96.5 + 1.80417 * A + 0.895833 * B - 0.0541667 * C - 1.49583 * D + 0.19375 * A*B + 0.00625 * A*C + 0.13125 * A*D - 0.08125 * B*C + 0.14375 * B*D - 0.01875 * C*D -2.80104 * A*A - 2.42604 * B*B - 5.16354 * C*C - 1.17604 * D*D ...(10)

## ANOVA (Analysis of Variance)

The ANOVA findings (Table 4) validate the statistical relevance of the quadratic model used in this study. A large F-value of 446.39 and a p-value of less than 0.0001 indicate the model's strong predictive power and suitability. Among the linear factors, agitation time (A), adsorbent dosage (B), and initial MG concentration (D) significantly affected the efficiency ($p < 0.0001$). However, pH (C) showed no notable influence on the process, with a p-value of 0.8893, suggesting a limited role in the studied range. The interaction terms (AC, AB, AD, BD, BC, and CD) also returned p-values greater than 0.05, indicating that the combined effects of these variables were statistically insignificant. In contrast, the quadratic terms ($A^2$, $B^2$, $C^2$, and $D^2$) were all highly significant ($p < 0.0001$), implying a pronounced curvature and a non-linear relationship between the factors and response. The lack of fit was statistically insignificant ($p > 0.05$), and a good $R^2$ value (0.9974) confirmed a strong agreement between the experimental data and model predictions, explaining over 99% of the variation in MG (Table 5).

## RSM Plots and Interaction

To assess MG dye adsorption onto Zn/Al@BOI, 3D plots were employed to examine the influences of agitation time, adsorbent dose, pH, and adsorbate concentration. As illustrated in Fig. 8(a) and 8(b), increasing the agitation time enhanced MG removal, likely owing to the greater number of active binding regions early in the process. The adsorption approached equilibrium after 30 min as these sites became increasingly occupied by the adsorbate. The pH also played a key role, with MG removal increasing from acidic to near-neutral pH and peaking at pH 8, as shown in Fig. 8(a) and 8(d). Under strongly acidic conditions, $H^+$ ions likely compete with dye molecules for active sites, thereby diminishing the uptake ability. At elevated pH levels, the deprotonation of surface groups can lead to electrostatic repulsion, slightly lowering the dye uptake. Fig. 8(c) shows the interaction between the dosage and dye concentration. While higher dosages improved removal due to more surface sites, increasing dye concentration (Fig. 8b, 8c) led to decreased efficiency as the sites became saturated. This highlights the need to balance the dosage with the pollutant load. Overall, the response plots revealed that all parameters influenced each other and must be optimized collectively for efficient MG degradation.

## Optimization

This study aimed to establish the optimal inputs for maximum MG degradation using the Design-Expert 13 software. The suggested parameters like agitation time of 33.1 min, nanocomposite dosage of 0.3 $g.L^{-1}$, pH 7.9, and adsorbate MG concentration of 20 $mg.L^{-1}$, predicted a removal efficiency of 96.87% with a desirability of 0.994 (Fig. 9). Experimental validation under the given inputs closely matched the calculated outcomes, confirming the accuracy of the model.

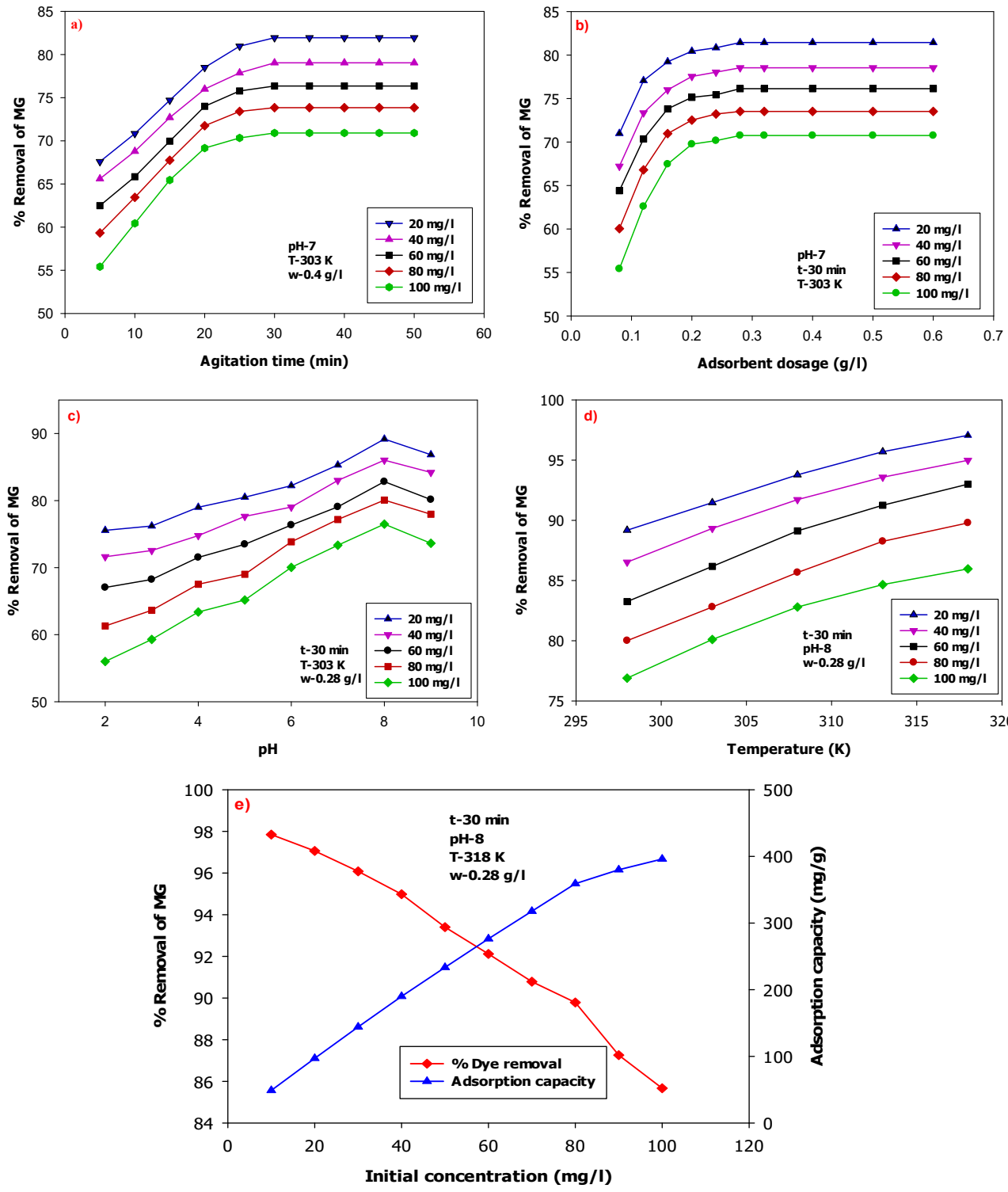


Fig. 7: Optimization of key operational variables on MG by Zn/Al@BOI: (a) time, (b) dosage, (c) pH, (d) temperature, and (e) initial concentration vs. $q_e$.

Table 3: Factors designed using CCD.

| Run | A:Time (min) | B:Dose [$g.L^{-1}$] | C:pH | D:Concentration [$mg.L^{-1}$] | MG Removal efficiency % |
|---|---|---|---|---|---|
| 1 | 30 | 0.3 | 8 | 20 | 96.5 |
| 2 | 40 | 0.2 | 7 | 25 | 84 |
| 3 | 30 | 0.3 | 6 | 20 | 76 |
| 4 | 40 | 0.4 | 9 | 15 | 89 |
| 5 | 20 | 0.2 | 9 | 25 | 80.4 |
| 6 | 30 | 0.3 | 10 | 20 | 76.1 |
| 7 | 10 | 0.3 | 8 | 20 | 82 |
| 8 | 30 | 0.3 | 8 | 20 | 96.5 |
| 9 | 20 | 0.2 | 7 | 25 | 80.5 |
| 10 | 20 | 0.4 | 9 | 15 | 85 |
| 11 | 40 | 0.2 | 7 | 15 | 87 |
| 12 | 50 | 0.3 | 8 | 20 | 89 |
| 13 | 30 | 0.1 | 8 | 20 | 85.5 |
| 14 | 40 | 0.2 | 9 | 15 | 87 |
| 15 | 40 | 0.2 | 9 | 25 | 84 |
| 16 | 30 | 0.3 | 8 | 20 | 96.5 |
| 17 | 20 | 0.4 | 7 | 25 | 82.4 |
| 18 | 20 | 0.4 | 7 | 15 | 85.5 |
| 19 | 20 | 0.2 | 7 | 15 | 84 |
| 20 | 20 | 0.4 | 9 | 25 | 82.2 |
| 21 | 30 | 0.5 | 8 | 20 | 88.5 |
| 22 | 40 | 0.4 | 7 | 15 | 89.1 |
| 23 | 30 | 0.3 | 8 | 20 | 96.5 |
| 24 | 30 | 0.3 | 8 | 20 | 96.5 |
| 25 | 30 | 0.3 | 8 | 20 | 96.5 |
| 26 | 30 | 0.3 | 8 | 20 | 96.5 |
| 27 | 40 | 0.4 | 7 | 25 | 86.9 |
| 28 | 20 | 0.2 | 9 | 15 | 84 |
| 29 | 30 | 0.3 | 8 | 10 | 95 |
| 30 | 30 | 0.3 | 8 | 30 | 89 |
| 31 | 40 | 0.4 | 9 | 25 | 86.3 |

## Adsorption Isotherms

The adsorption of MG onto Zn/Al@BOI was evaluated using the Langmuir and Freundlich isotherm models (Fig. 10a–b). The Langmuir model ($R^2 = 0.9787$) describes uniform surface adsorption, a monolayer of adsorbate molecules, with a high maximum capacity of 376 $mg.g^{-1}$, likely due to electrostatic interactions and active surface sites. However, the Freundlich model showed an even better fit ($R^2 = 0.9957$), indicating non-uniform surface characteristics that support multi-layer adsorption. The Freundlich constant ($n = 1.9055$) confirmed the favorable adsorption. These results imply that while Langmuir highlights high capacity, the Freundlich model more accurately describes the adsorption behavior of the doped bio-waste-based material (Sowjanya et al. 2023, Ratnam et al. 2022)

## Adsorption Kinetics

To elucidate the nature of the adsorption interaction kinetics of MG onto Zn/Al@BOI, the observed data were interpreted through pseudo-first- and second-order models (Fig. 10c–d), with the corresponding kinetic parameters listed in Table 6. The pseudo-first-order model (Fig. 10c) offered a weaker correlation ($R^2 = 0.8920$), indicating limited suitability. Conversely, the pseudo-$2^{nd}$-order model (Fig. 10d) modeled the data exceptionally well ($R^2 = 0.9998$), highlighting chemisorption as the dominant mechanism. This suggests

Table 4: ANOVA Output for the Fitted Quadratic Model.

| Source | Sum of Squares | df | Mean Square | F-value | p-value | |
|---|---|---|---|---|---|---|
| **Model** | 1171.46 | 14 | 83.68 | 446.39 | < 0.0001 | significant |
| A-Time | 74.55 | 1 | 74.55 | 397.73 | < 0.0001 | |
| B-Dosage | 21.09 | 1 | 21.09 | 112.53 | < 0.0001 | |
| C-pH | 0.0038 | 1 | 0.0038 | 0.0200 | 0.8893 | |
| D-Concentration | 69.70 | 1 | 69.70 | 371.84 | < 0.0001 | |
| AB | 0.2756 | 1 | 0.2756 | 1.47 | 0.2429 | |
| AC | 0.0506 | 1 | 0.0506 | 0.2701 | 0.6104 | |
| AD | 0.6006 | 1 | 0.6006 | 3.20 | 0.0924 | |
| BC | 0.0056 | 1 | 0.0056 | 0.0300 | 0.8646 | |
| BD | 0.1056 | 1 | 0.1056 | 0.5635 | 0.4638 | |
| CD | 0.1056 | 1 | 0.1056 | 0.5635 | 0.4638 | |
| $A^2$ | 229.39 | 1 | 229.39 | 1223.76 | < 0.0001 | |
| $B^2$ | 172.67 | 1 | 172.67 | 921.16 | < 0.0001 | |
| $C^2$ | 771.68 | 1 | 771.68 | 4116.77 | < 0.0001 | |
| $D^2$ | 26.21 | 1 | 26.21 | 139.80 | < 0.0001 | |
| **Residual** | 3.00 | 16 | 0.1874 | | | |
| Lack of Fit | 3.00 | 10 | 0.2999 | | | |
| Pure Error | 0.0000 | 6 | 0.0000 | | | |
| **Cor Total** | 1174.46 | 30 | | | | |

that the adsorption process involves electron sharing or exchange through valence forces, with surface complexation or ion exchange as the rate-determining step. This behavior aligns with the highly active and heterogeneous surface of Zn/Al@BOI, making it efficient for MG removal (Ratnam et al. 2022, Subhashita et al. 2022).

### Thermodynamic studies

The thermodynamic variables for MG removal onto Zn/Al@BOI were determined using the van't Hoff plot (Fig. 10e), which exhibited strong linearity ($R^2 = 0.9716$), confirming a clear temperature dependence. The enthalpy change ($\Delta H^\circ$ = +23.82 kJ.moL$^{-1}$) suggests that the process is endothermic, likely involving chemisorption or diffusion through pores. An entropy change ($\Delta S^\circ$ = +103.49 J/(mol·K$^{-1}$)) signifies enhanced disorder at the adsorbent–MG dye boundary, possibly owing to moisture evaporation and the rearrangement of the adsorbate structure. Gibbs free energy outcomes ($\Delta G^\circ$ = –8.57– ,9.10, and –8.10 kj.moL$^{-1}$ at 318, 313, and 308 K, respectively) confirm the spontaneity and thermodynamic favorability of the process. The improved removal at higher temperatures may result from enhanced dye molecule mobility and easier access to active binding sites on the adsorbent (Sowjanya et al. 2023, Ratnam et al. 2022, Subhashita et al. 2022).

Table 5: Model fit evaluation criteria.

| | |
|---|---|
| Std. Dev. | 0.4330 |
| Mean | 87.64 |
| C.V. % | 0.4940 |
| $R^2$ | 0.9974 |
| Adjusted $R^2$ | 0.9852 |
| Predicted $R^2$ | 0.9753 |
| Adeq Precision | 59.0789 |

## CONCLUSIONS

In this study, a green co-precipitation approach was utilized to synthesize a zinc and aluminum dual-doped nanocomposite derived from Brassica oleracea var. italica stem bio-waste (Zn/Al@BOI) for efficient malachite green (MG). Characterization analyses, including SEM-EDX, XRD, FTIR, XPS, TGA, and BET, revealed a well-developed crystalline structure, heterogeneous surface morphology,

Table 6: Kinetic variables of removal of MG onto Zn/Al@BOI.

| S.No | Model | Parameters |
|---|---|---|
| 1. | Pseudo-1$^{st}$ -order model | $q_e$=43.77 mg.g$^{-1}$<br>$R^2$=0.8920 |
| 2. | Pseudo -2$^{nd}$ -order model | $q_e$= 444 mg.g$^{-1}$<br>$R^2$=0.9998 |
| 3. | Elovich model | $R^2$=0.9115 |
| 4. | Intra-particle diffusion | $R^2$=0.92 |

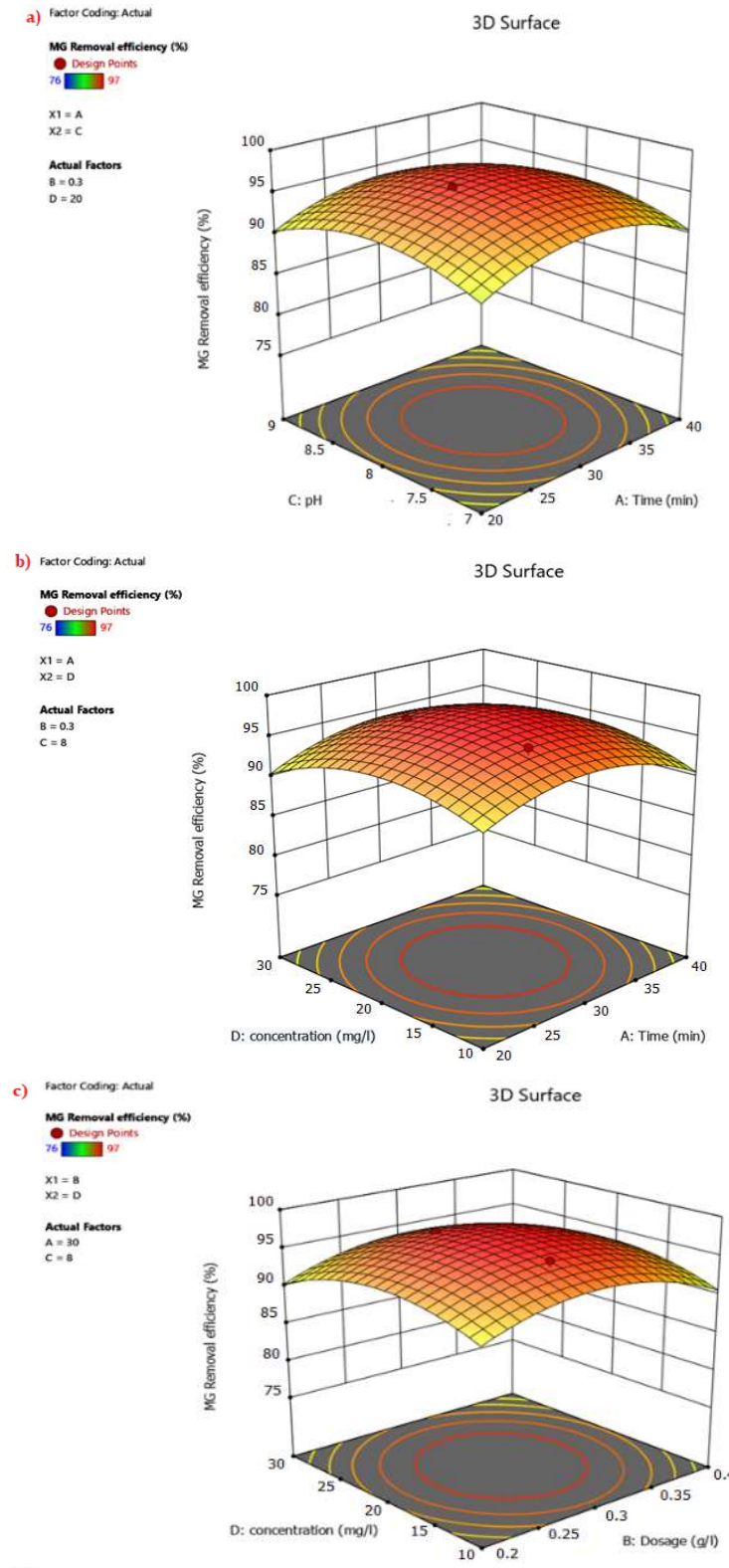
a)
Factor Coding: Actual
MG Removal efficiency (%)
Design Points
76
97
X1 = A
X2 = C
Actual Factors
B = 0.3
D = 20
3D Surface
MG Removal efficiency (%)
C: pH
A: Time (min)
b)
Factor Coding: Actual
MG Removal efficiency (%)
Design Points
76
97
X1 = A
X2 = D
Actual Factors
B = 0.3
C = 8
3D Surface
MG Removal efficiency (%)
D: concentration (mg/l)
A: Time (min)
c)
Factor Coding: Actual
MG Removal efficiency (%)
Design Points
76
97
X1 = B
X2 = D
Actual Factors
A = 30
C = 8
3D Surface
MG Removal efficiency (%)
D: concentration (mg/l)
B: Dosage (g/l)

Figure Cont....

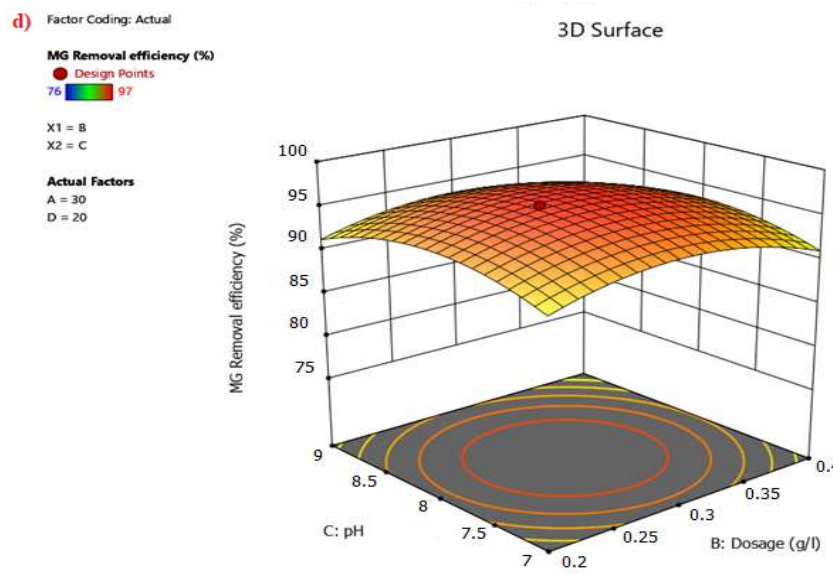


Fig. 8: Three-dimensional surface graphs showing the combined effects of key inputs on the adsorption of the adsorbate onto Zn/Al@BOI: (a) solution pH and time, (b) adsorbate concentration and time, (c) concentration and nanocomposite dosage, and (d) pH and dosage.

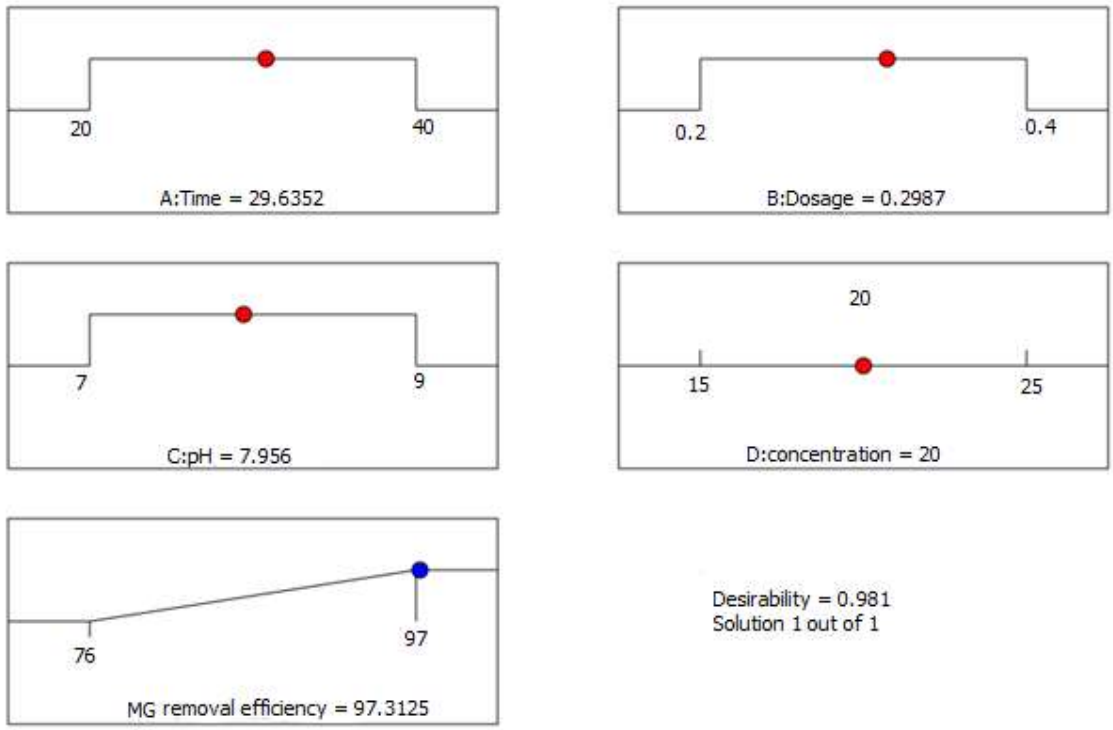


Fig. 9: Ramp plot of the optimization.

excellent thermal stability, and a marked surface area of 80.53 $m^2$. $g^{-1}$. EDX and XPS analyses confirmed the integration of Zn and Al into the bio-waste matrix, while the FT-IR spectra highlighted the functional groups involved in dye interactions. Process input optimization was carried out using RSM with a CCD, identifying ideal conditions: agitation time of 29.64 min, dose of 0.2987 $g.L^{-1}$, pH 7.96, and MG concentration of 20 $mg.L^{-1}$, resulting in 97.31%

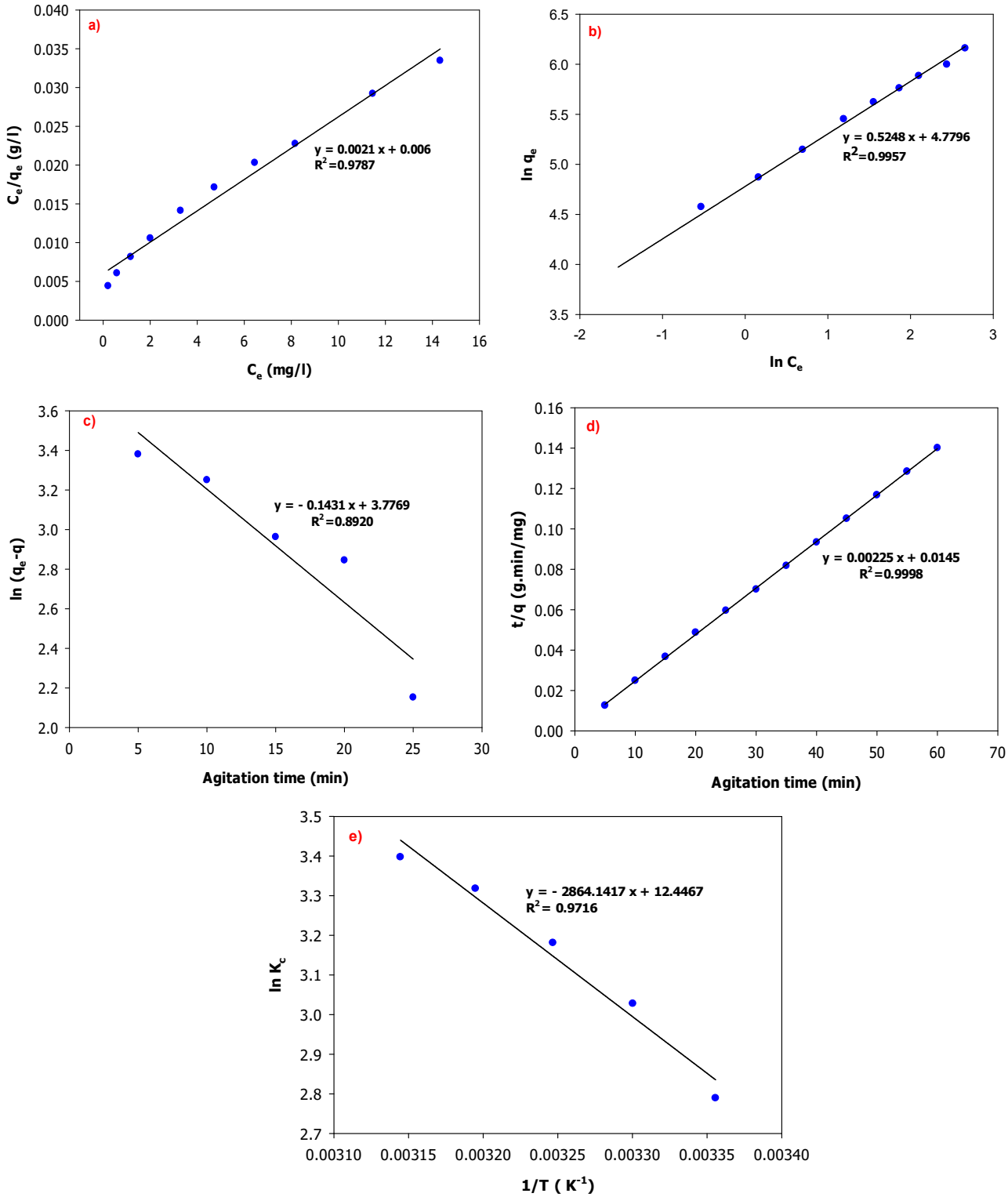


Fig. 10: (a) Langmuir isotherm, (b) Freundlich isotherm, (c) pseudo-1st order model, (d) pseudo-2nd order model, and (e) Van't Hoff plot for MG uptake onto Zn/Al@BOI.

removal under optimized inputs. The Langmuir isotherm estimated a maximum uptake capacity of 336 $mg.g^{-1}$, that closely matched the experimental result of around 356 $mg.g^{-1}$. Kinetic studies noted that the adsorption followed a pseudo-2nd-order model, while thermodynamic studies confirmed that the approach was spontaneous, endothermic, and primarily driven by physisorption. These results highlight Zn/Al@BOI as an efficient, sustainable, and affordable water purification material.

## ACKNOWLEDGMENTS

The authors sincerely thank the Department of Chemical Engineering, AU College of Engineering, for providing the necessary research facilities and academic support throughout the study.

## REFERENCES

Ananda, A., Ramakrishnappa, T., Ravishankar, T.N., Reddy Yadav, L.S. and Jayanna, B.K., 2023. RSM-BBD optimization approach for degradation and electrochemical sensing of Evan's blue dye using green synthesized $ZrO_2$–ZnO nanocomposite. *Inorganic and Nano-Metal Chemistry*, 53(1), pp.123-130. [DOI]

Ashraf, I., Singh, N.B. and Agarwal, A., 2023. Green synthesis of iron oxide nanoparticles using Amla seed for methylene blue from water. *Materials Today Proceedings*, 72(1), pp.311-316. [DOI]

Aziz, T., Farid, A., Chinnam, S., Haq, F., Kiran, M., Wani, A.W. and Akhtar, M.S., 2023. Modified cellulose nanocrystals for cationic dye adsorption. *Chemosphere*, 321(1), pp.137999. [DOI]

Banerjee, S. and Chattopadhyaya, M.C., 2017. Tartrazine removal from aqueous solutions using agricultural by-products. *Arabian Journal of Chemistry*, 10(1), pp.S1629-S1638. [DOI]

Bilal, M., Ihsanullah, I., Shah, M.U.H., Reddy, A.V.B. and Aminabhavi, T.M., 2022. Recent advances in the removal of dyes from wastewater using low-cost adsorbents. *Journal of Environmental Management*, 321(1), pp.115981. [DOI]

Chan, Y.Y., Pang, Y.L., Lim, S. et al. 2020. Biosynthesized Fe- and Ag-doped ZnO nanoparticles using Clitoria ternatea Linn extract for Congo red degradation. *Environmental Science and Pollution Research*, 27(1), pp.34675-34691. [DOI]

Çifçi, D.İ. and Aydın, N., 2022. Magnetic iron-doped filtered coffee bio-waste-based carbon for the adsorption of reactive blue 21. *Journal of Water Chemistry and Technology*, 44(1), pp.317-326. [DOI]

Debord, J., Harel, M., Bollinger, J.C. and Chu, K.H., 2022. The Elovich isotherm equation: Back to the roots and new developments. *Chemical Engineering Science*, 262(1), pp.118012. [DOI]

Dharmarathna, S.P. and Priyantha, N., 2024. Investigation of boundary layer effect of intra-particle diffusion on methylene blue adsorption. *Energy Nexus*, 14(1), pp.100294. [DOI]

Dutta, S., Gupta, B., Srivastava, S.K. and Gupta, A.K., 2021. Recent advances on the removal of dyes from wastewater using various adsorbents: A critical review. *Materials Advances*, 2(1), pp.4497-4531. [DOI]

El Naeem, G.A., Abd-Elhamid, A.I., Farahat, O.O., El-Bardan, A.A., Soliman, H.M. and Nayl, A.A., 2022. Crystal violet and methylene blue adsorption using sugarcane bagasse cellulose adsorbent. *Journal of Materials Research and Technology*, 19(1), pp.3241-3254. [DOI]

El Ouadhriri, F., Adachi, A., Elyemni, M., Bayout, A., Hmamou, A., Bendaoud, A. and Lahkimi, A., 2022. N, P-dually doped carbocatalyst from olive pomace obtained by hydrothermal carbonization. *Journal of Environmental Chemical Engineering*, 10(1), pp.108449. [DOI]

Elizalde-González, M.P., Geyer, W., Guevara-Villa, M.R., Mattusch, J., Peláez-Cid, A.A. and Wennrich, R., 2006. Maize waste adsorbent for textile. *Colloids and Surfaces A: Physicochemical and Engineering Aspects*, 278(1), pp.89-97. [DOI]

Granado-Castro, M.D., Galindo-Riaño, M.D., Gestoso-Rojas, J., Sánchez-Ponce, L., Casanueva-Marenco, M.J. and Díaz-de-Alba, M., 2024. Ecofriendly application of calabrese broccoli stalk waste for $Pb^{2+}$ removal. *Agronomy*, 14(1), pp.554. [DOI]

Ho, Y.S. and McKay, G., 1999. Pseudo-second order model for sorption processes. *Process Biochemistry*, 34(1), pp.451-465. [DOI]

Inobeme, A., Mathew, J.T., Adetunji, C.O., Agbugui, M.O., Inobeme, J., Enerijiofi, K.E. and Daniel, O., 2024. Understanding Dye Pollution and Its Impact on the Environment. In: *Dye Pollution from Textile Industry*. Springer, Singapore, pp.3-15. [DOI]

Javadian, H., Angaji, M.T. and Naushad, M., 2014. Polyaniline/γ-alumina nanocomposite for anionic dye adsorption. *Journal of Industrial and Engineering Chemistry*, 20(1), pp.3890-3900. [DOI]

Jha, A. and Mishra, S., 2024. Exploring the potential of waste biomass-derived pectin and its functionalized derivatives for water treatment. *International Journal of Biological Macromolecules*, 275(1), pp.133613. [DOI]

Kacan, E., 2016. Activated carbon from textile sludge for. *Journal of Environmental Management*, 166(1), pp.116-123. [DOI]

Karthikeyan, N. and Vijayalakshmi, K.A., 2024. The Effective Capacitance Behaviour of Argon Plasma Exposed Al Dopped CdO Electrode Used in Efficient Metal-Air Batteries. *ChemistrySelect*, *9*(28), p.e202401617. [DOI]

Karunakaran, G., Cho, E.B., Kumar, G.S., Kolesnikov, E., Govindaraj, S.K., Mariyappan, K. and Boobalan, S., 2023. CTAB enabled microwave-hydrothermal assisted mesoporous Zn-doped hydroxyapatite nanorods synthesis using bio-waste Nodipecten nodosus scallop. *Environmental Research*, 216(1), pp.114683. [DOI]

Klett, C., Barry, A., Balti, I., Lelli, P., Schoenstein, F. and Jouini, N., 2014. Nickel-doped ZnO for methyl orange and tartrazine adsorption. *Journal of Environmental Chemical Engineering*, 2(1), pp.914-926. [DOI]

Li, X., Wang, Z., Ning, J., Gao, M., Jiang, W., Zhou, Z. and Li, G., 2018. Polyethyleneimine-modified persimmon tannin bioadsorbent for anionic dye adsorption. *Journal of Environmental Management*, 217(1), pp.305-314. [DOI]

Liu, J., Wang, N., Zhang, H. and Baeyens, J., 2019. Adsorption of Congo red dye on $FexCo_{3-x}O_4$ nanoparticles. *Journal of Environmental Management*, 238(1), pp.473-483. [DOI]

Mall, I.D., Srivastava, V.C., Kumar, G.V.A. and Mishra, I.M., 2006. Mesoporous fertilizer plant waste carbon for dye adsorption. *Colloids and Surfaces A: Physicochemical and Engineering Aspects*, 278(1), pp.175-187. [DOI]

Manojkumar, U., Kaliannan, D., Srinivasan, V., Balasubramanian, B., Kamyab, H., Mussa, Z.H., Palaniyappan, J., Mesbah, M., Chelliapan, S. and Palaninaicker, S., 2023. Green synthesis of zinc oxide nanoparticles using Brassica oleracea var. botrytis leaf extract. *Chemosphere*, 323(1), pp.138204. [DOI]

Monvisade, P. and Siriphannon, P., 2009. Chitosan intercalated montmorillonite for cationic dye adsorption. *Applied Clay Science*, 42(1), pp.427-431. [DOI]

Ouassif, H., Moujahid, E.M., Lahkale, R., Sadik, R., Bouragba, F.Z., Sabbar, E.M. and Diouri, M., 2020. Zinc–aluminum layered double hydroxide for tartrazine. *Surfaces and Interfaces*, 18(1), pp.100401. [DOI]

Parveen, K. and Rafique, U., 2018. Cobalt-doped alumina hybrids for textile effluent adsorption. *Adsorption Science and Technology*, 36(1), pp.182-197. [DOI]

Poiba, V.R., Sowjanya, B., King, P. and Vangalapati, M., 2023. Removal of methylene blue dye by using synthesised Grevillea robusta silver

nanoparticles. *Advances in Materials and Processing Technologies*, 9(1), pp.1-15. [DOI]

Polipalli, K. and Pulipati, K., 2013. Equilibrium, kinetic and thermodynamic studies of biosorption of methylene blue dye using plant biomass as biosorbent. *International Journal of Scientific and Engineering Research*, 4(1), pp.1244-1252.

Raj, R.M., Ganesan, S., Suganthi, S., Vignesh, S., Hatamleh, A.A., Alnafisi, B.K. and Lo, H.M., 2023. Zinc–aluminium polymeric framework for drug and. *Chemosphere*, 311(1), pp.137105. [DOI]

Ratnam, M.V., Vangalapati, M., Rao, K.N. and Chandra, K.R., 2022. Efficient removal of methyl orange using MgO nanoparticles loaded onto activated carbon. *Bulletin of the Chemical Society of Ethiopia*, 36(3), pp.531-544. [DOI]

Raval, N.P., Shah, P.U. and Shah, N.K., 2017. Malachite green 'a cationic dye' and its removal from aqueous solution by adsorption. *Applied Water Science*, 7(1), pp.3407-3445. [DOI]

Shindhal, T., Rakholiya, P., Varjani, S., Pandey, A., Ngo, H.H., Guo, W. and Taherzadeh, M.J., 2021. A critical review on advances in the practices and perspectives for the treatment of dye industry wastewater. *Bioengineered*, 12(1), pp.70-87. [DOI]

Sowjanya, B., King, P. and Meena, V., 2023. Skin of Allium sativum mediated green synthesis of ZnO nanoparticles for Congo red. *European Chemical Bulletin*, 13(5), pp.326-332. [DOI]

Sowjanya, B., King, P., Vangalapati, M. and Myneni, V.R., 2023. Copper doped zinc oxide nanoparticles: Synthesis, characterization, and application for adsorptive removal of toxic azo dye. *International Journal of Chemical Engineering*, 2023(1), pp.8640288. [DOI]

Sowjanya, B., Sirisha, U., Juttuka, A.S., Matla, S., King, P. and Vangalapati, M., 2022. Synthesis and characterization of zinc oxide nanoparticles: Application for alizarin red S. *Materials Today Proceedings*, 62(1), pp.3968-3972. [DOI]

Subhashita, M., Punugoti, T., Sowjanya, B., Poiba, V.R. and Vangalapati, M., 2022. Synthesis of Cu/ZnO nanoparticles and their use for Cetrimonium Bromide removal. *Advances in Materials and Processing Technologies*, 8(1), pp.1880-1888. [DOI]

Tajat, N., El Hayaoui, W., Bougdour, N., Idlahcen, A., Radaa, C., Bakas, I. and Qourzal, S., 2022. Utilization of Zn–Al–Cl layered double hydroxide as an adsorbent for the removal of anionic dye Remazol Red 23. *Nanotechnology for Environmental Engineering*, 7(1), pp.343-357. [DOI]

Velusamy, S., Kandasamy, K., Kuppusamy, M.R., Manikandan, M., Velusami, N. and Govindasamy, K., 2025. Eco-friendly green synthesis: Harnessing Ni/Al-layered double hydroxide-activated carbon nanocomposite. *International Journal of Environmental Research*, 19(1), pp.1-18. [DOI]

Verma, A., Thakur, S., Mamba, G., Gupta, R.K., Thakur, P. and Thakur, V.K., 2020. Graphite modified sodium alginate hydrogel composite for efficient removal of malachite green dye. *International Journal of Biological Macromolecules*, 148(1), pp.1130-1139. [DOI]

Youssef, A.M., Moustafa, H.A., Barhoum, A., Hakim, A.E.F.A. and Dufresne, A., 2017. Polyaniline nanocomposite based on Zn/Al-LDHs: Morphological, electrical and antibacterial evaluation. *ChemistrySelect*, 2(1), pp.8553-8566. [DOI]

Zhang, H., Xing, L., Liang, H., Ren, J., Ding, W., Wang, Q. and Xu, C., 2022. Efficient removal of Remazol Brilliant Blue R from water by a cellulose-based activated carbon. *International Journal of Biological Macromolecules*, 207(1), pp.254-262. [DOI]